

Demonstration of geometric diabatic control of quantum states

Kento Sasaki ^{*} and Yuki Nakamura 

Department of Physics, The University of Tokyo, Bunkyo-ku, Tokyo 113-0033, Japan

Tokuyuki Teraji 

National Institute for Materials Science, Tsukuba, Ibaraki 305-0044, Japan

Takashi Oka 

The Institute for Solid State Physics, The University of Tokyo, Kashiwa, Chiba 277-8581, Japan

Kensuke Kobayashi [†]

*Department of Physics, The University of Tokyo, Bunkyo-ku, Tokyo 113-0033, Japan;
Institute for Physics of Intelligence, The University of Tokyo, Bunkyo-ku, Tokyo 113-0033, Japan;
and Trans-scale Quantum Science Institute, The University of Tokyo, Bunkyo-ku, Tokyo 113-0033, Japan*

 (Received 22 November 2022; revised 17 March 2023; accepted 27 April 2023; published 26 May 2023)

Geometric effects can play a pivotal role in streamlining quantum manipulation. We demonstrate a geometric diabatic control, that is, perfect tunneling between spin states in a diamond by a quadratic sweep of a driving field. The field sweep speed for the perfect tunneling is determined by the geometric amplitude factor and can be tuned arbitrarily. Our results are obtained by testing a quadratic version of Berry's twisted Landau-Zener model. This geometric tuning is robust over a wide parameter range. Our work provides a basis for quantum control in various systems, including condensed-matter physics, quantum computation, and nuclear magnetic resonance.

DOI: [10.1103/PhysRevA.107.053113](https://doi.org/10.1103/PhysRevA.107.053113)

Tunneling is an exotic yet ubiquitous quantum phenomenon. To control quantum states, a common strategy known as adiabatic control avoids it by moving a large energy barrier slowly. Another ubiquitous feature of quantum physics is geometric effects [1]. A well-known example is the geometric phase [2] that a particle acquires during an adiabatic motion. However, geometric effects are not restricted by adiabaticity. Even during diabatic tunneling events, geometric effects take place and lead to grave consequences in the dynamics.

The simplest system that demonstrates the marriage of tunneling and geometric effects is the twisted Landau-Zener (TLZ) model introduced by Berry, which describes a particle in two quantum states driven by an external field [3]. In the original untwisted Landau-Zener (LZ) model [4–7], when two energy levels change in time, quantum tunneling across an energy gap Δ occurs depending on the speed of the change [Fig. 1(a)] [8,9]. The tunneling probability P depends on the sweep speed F [Fig. 1(c)]; $P = 0$ in the adiabatic limit ($F \rightarrow 0$), while P is unity in the diabatic limit ($|F| \rightarrow \infty$). Such speed-dependent tunneling has been demonstrated in various systems [10–16]. In the TLZ model, the driving field has a twist and the adiabatic to diabatic transition is geometrically modulated [17,18]. Recently, the importance of the geometric effects was recognized not only in equilibrium [19]

but also in nonequilibrium [20–23]. The TLZ model, which possesses a new nonequilibrium tuning knob on top of the LZ model, should be widely applied to materials engineering [24,25] and quantum controls [26–29]. Despite a few experiments [30–33], the opportunity to utilize such geometric tuning for quantum control has long been overlooked, and its robustness remains unexplored.

Here, using an electron spin in a diamond, we realize and test an ideal TLZ model with a quadratic twist [24] that manifests perfect tunneling and nonreciprocity over a wide range of gap and twist parameters. We measure the tunneling probabilities with high precision and obtain an average of 95.5% under the condition where perfect tunneling occurs. The condition of perfect tunneling can be smoothly tuned by adjusting the curvature of the quadratic sweep. These geometrical effects are robust beyond the framework of the existing theory [24]. This geometric diabatic control is ubiquitous and can be applied to various quantum systems.

As a geometric diabatic control, we aim to realize perfect tunneling ($P = 1$) and change the state at the same time. The Hamiltonian for the TLZ model in the natural units is defined as [24]

$$\hat{H} = \mathbf{b} \cdot \hat{\boldsymbol{\sigma}} = m\hat{\sigma}_x + vq\hat{\sigma}_y + \frac{1}{2}\kappa_{\parallel}v^2q^2\hat{\sigma}_z, \quad (1)$$

where $\hat{\sigma}_j$ ($j = x, y,$ and z) is the Pauli operator and $\mathbf{b} = (b_x, b_y, b_z) \equiv (m, vq, 1/2\kappa_{\parallel}v^2q^2)$ is a driving field. We change the parameter q in time as $q = -F(t - T/2)$ between time $t = 0$ and $t = T$ with a dimensionless sweep speed F . This is a quadratic version of the original TLZ model [3];

*kento.sasaki@phys.s.u-tokyo.ac.jp

†kensuke@phys.s.u-tokyo.ac.jp

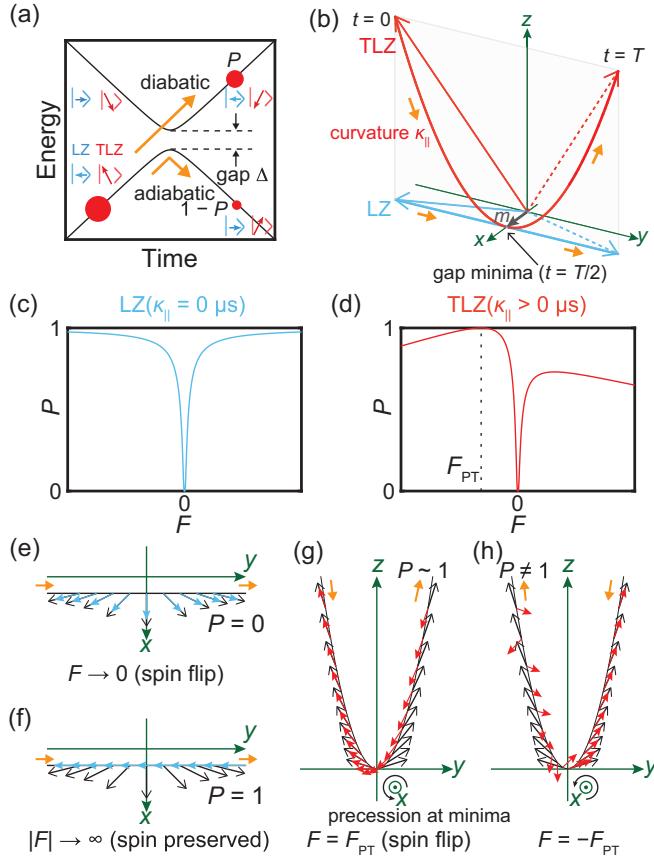


FIG. 1. Comparison of the Landau-Zener (LZ) transition and the twisted Landau-Zener (TLZ) transition. (a) Tunneling at level anticrossing. (b) Sweeping of the driving field. The fields at $t = 0$ and $t = T$ for the LZ (TLZ) model are indicated by solid and dashed blue (red) arrows, respectively. Predicted (c) LZ transition probability and (d) TLZ transition probability are plotted as a function of the speed F . Dynamics of the field (black arrow) and spin (blue arrow) in the LZ model are plotted in the (e) adiabatic and (f) diabatic limits [see also (b) and (c)]. Dynamics of the field (black arrow) and spin (red arrow) in the TLZ model are plotted at (g) $F = F_{\text{PT}}$ and (h) $F = -F_{\text{PT}}$ [see also (b) and (d)]. The solid black line indicates the field amplitude in the xy plane in (e) and (f) and in the yz plane in (g) and (h). The origin of each arrow corresponds to the field amplitude at each instant.

$\Delta = 2m$ is the gap and $2v (>0)$ is the energy slope. Figure 1(b) depicts the initial and final fields as a solid red arrow ($t = 0$) and a red dotted arrow ($t = T$), respectively. The b_z component, which depends quadratically on time, induces a twist of the field. This twist appears in the trajectory of the field [the red solid line in Fig. 1(b)] and its strength is determined by the geodesic curvature $\kappa_{||}$. Situations in which the spin and driving field are always kept parallel or antiparallel are adiabatic; situations that deviate from this are diabatic. The diabatic geometric effect is captured by the geometric amplitude factor [3] (also known as the quantum geometric potential [17] or shift vector [25]) $R_{12}(q) = -A_{11}(q) + A_{22}(q) + \partial_q \arg A_{12}(q)$, where the Berry connection is defined by $A_{ni}(q) = \langle n(q) | i \partial_q | l(q) \rangle$ using the instantaneous eigenstate $|n(q)\rangle$ satisfying $\hat{H}(q)|n(q)\rangle = E_n(q)|n(q)\rangle$. The

tunneling probability P from $|1\rangle$ to $|2\rangle$ is given by [24]

$$P \approx \exp \left[-\frac{\pi}{4v|F|} \left(\Delta + \frac{FR_{12}(0)}{2} \right)^2 \right], \quad (2)$$

where $R_{12}(0) = v\kappa_{||}$ holds in the present model. Equation (2), referred to as the TLZ formula in this work, is derived using a twisting coordinate transformation [24] and it recovers the LZ formula when $\kappa_{||} = 0$ [Fig. 1(c)]. We stress that the TLZ formula is approximate in contrast to the LZ formula, which is asymptotically exact. Figure 1(d) shows the behavior of the transition described by the TLZ formula when $\kappa_{||} > 0$. The P is nonreciprocal to the sign reversal of the speed F corresponding to the field sweep direction [25]. In Eq. (2), the gap Δ in the LZ model is effectively shifted to $\Delta + \frac{FR_{12}(0)}{2}$ by the geometric amplitude factor [17,24]. In particular, when the speed is

$$F_{\text{PT}} = -2\Delta/R_{12}(0) \quad (3)$$

the effective gap closes and the tunneling probability saturates $P \approx 1$. We call this behavior perfect tunneling (PT) [24], and the speed at which P is maximized is referred to as the PT condition. In contrast to the LZ case, the quantum state changes during the diabatic transition from the initial state $|1(q = FT/2)\rangle$ to the final state $|2(q = -FT/2)\rangle$ and thus allows us to realize geometric diabatic control of the quantum states. Our main purpose is to extensively test the behaviors predicted by the TLZ formula [Eq. (2)].

We realize the TLZ transition with an electron spin of a single nitrogen-vacancy (NV) center in a diamond [12,13,34]. We use the NV center's $m_S = 0$ and -1 states as a two-level system and manipulate it with microwave pulses. In a suitable rotating frame (see the Supplemental Material [35]), the Hamiltonian is expressed as (\hat{S}_i denotes the $S = \frac{1}{2}$ spin operators)

$$\hat{H}_r = f_R [\cos(\phi_{\text{mw}}) \hat{S}_x - \sin(\phi_{\text{mw}}) \hat{S}_y] + \frac{d(f_{\text{det}} t)}{dt} \hat{S}_z, \quad (4)$$

where f_R is the Rabi frequency corresponding to the microwave field amplitude, ϕ_{mw} is the microwave phase, and f_{det} is the detuning between the resonance frequency and the microwave frequency. We generate a microwave pulse satisfying $f_R = \sqrt{b_x^2 + b_y^2}$, $\phi_{\text{mw}} = -\arctan(b_y/b_x)$, and $f_{\text{det}} = \int_0^t b_z(t') dt'$ so that Eq. (4) reproduces the driving field \mathbf{b} in the TLZ Hamiltonian [Eq. (1)]. This conversion to the $S = \frac{1}{2}$ system in MKS units corresponds to making the following changes to each parameter: $m \rightarrow \pi m$, $v \rightarrow \pi v$, and $\kappa_{||} \rightarrow \kappa_{||}/\pi$ (see [35]). We adjust the sweep duration T considering the coherence time and available microwave parameter ranges. Figure 2(a) shows the measurement sequence. We use green laser pulses and photoluminescence (PL) measurements for spin initialization and readout. We prepare the initial and final states using rectangular microwave pulses after and before the laser pulse to match the instantaneous field direction with the projection direction. The obtained PL intensity is precisely converted to a tunneling probability using reference PL intensities of the $m_S = 0$ and -1 states [36].

We show our experimental results obtained when the gap parameter is fixed as $m = 0.5$ MHz. Without loss of

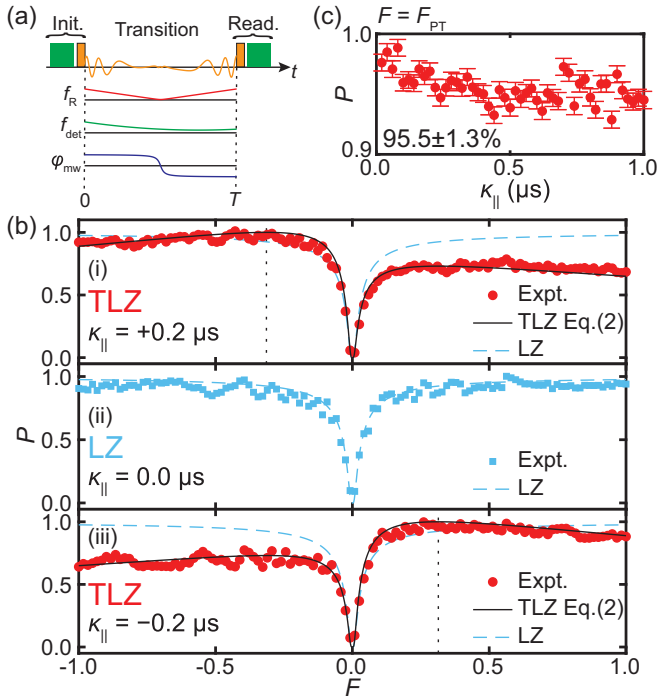


FIG. 2. Demonstration of the TLZ transition at $m = 0.5$ MHz. (a) Measurement sequence. Laser and microwave pulses are used for initialization and readout of the NV center. (b) Dependence of tunneling probability P on speed F . The squares and circles indicate experimental results, black solid lines indicate the TLZ formula [Eq. (2)], and vertical black dotted lines indicate $F = F_{PT}$. The blue dashed lines indicate the LZ formula [TLZ with $R_{12}(0) = 0$]. (c) Tunneling probability at $F = F_{PT}$ in the range of $\kappa_{\parallel} = 0-1 \mu\text{s}$. The error bars indicate 65% confidence intervals estimated from the shot noise of the PL measurement.

generality, we investigate the probability P [Eq. (2)] by selecting the energy slope v to $(10 \text{ MHz})^2$ and adjusting only the dimensionless speed F . First, we set $\kappa_{\parallel} = 0 \mu\text{s}$ to address the conventional LZ model. The blue circles in Fig. 2(b ii) show the experimental result. The lower the speed ($F \rightarrow 0$), the lower the transition probability P ; the behavior is symmetric between positive and negative speeds. It agrees well with the LZ formula (black solid line) and proves that our system reproduces the LZ model with high accuracy (for more details see [35]).

We then address the TLZ transition when $\kappa_{\parallel} = 0.2 \mu\text{s}$, shown in Fig. 2(b i). The experimental result (red circles) is asymmetric in $F \rightarrow -F$ and becomes higher for $F < 0$ than for $F > 0$. The P reaches maxima in the vicinity of the predicted PT condition ($F = F_{PT}$) indicated by the vertical dashed line. Specifically, as shown in Fig. 2(c), we find $P = 95.5 \pm 1.3\%$, on average, in a range of $\kappa_{\parallel} = 0.0-1.0 \mu\text{s}$. Figure 2(b iii) shows the results when $\kappa_{\parallel} = -0.2 \mu\text{s}$. Compared to the $\kappa_{\parallel} = 0.2 \mu\text{s}$ case [Fig. 2(b i)], it shows totally inverted behavior to the speed F . These behaviors are qualitatively different from the LZ transition (blue dashed line) and well reproduced by the TLZ formula without any adjustable parameters (black solid line). These are our central results, proving that the tunneling probability is successfully

modulated by the geodesic curvature κ_{\parallel} of the driving field, resulting in perfect tunneling and nonreciprocity. The fact that perfect tunneling, which has only been possible in the extremely fast speed limits of the LZ model, is achieved even at finite speeds is essentially different in the long history of the LZ physics.

Here we give an intuitive picture of the perfect tunneling phenomenon. Figure 1(g) shows the driving field (black arrow) and spin (red arrow) dynamics at $F = F_{PT}$. The quadratic sweep produces adiabatic dynamics in the initial stage ($t \sim 0$) and diabatic dynamics near the gap minima ($t \sim T/2$). Near the gap minima, the x component of the driving field \mathbf{b} , i.e., the gap itself ($b_x = m$), causes spin precession and rotates the spin around the x axis. When the PT condition is fulfilled, this rotation of the spin is synchronized with the counterclockwise twist of the field (also around the x axis) and the transition to the excited state is achieved smoothly. Thus a spin flipping is realized [Fig. 1(g)]. When the sweep direction is reversed ($F = -F_{PT}$), as shown in Fig. 1(h), the clockwise field twist cannot synchronize with the spin precession. This geometric motion near the gap minima increases the effective gap $\Delta + \frac{FR_{12}}{2}$ and prevents tunneling. More generally, the observed nonreciprocity is analogous to the well-known selective absorption of circularly polarized light, but in the nonperturbative regime.

As described above, the spin flips during the perfect tunneling. In terms of quantum control, a spin flip can also be achieved differently using the Rabi oscillation and the adiabatic control (or its shortcut [37]). The driving field and spin are orthogonal, parallel, and antiparallel in the Rabi oscillation, the adiabatic control, and the TLZ model, respectively. This difference in the restriction of the driving field to the spin direction makes a difference in control speed, robustness, and implementability. Our geometric diabatic control is an effective means of increasing the versatility of quantum control (see [35]).

Next we study the validity of the TLZ formula [Eq. (2)] when the twist becomes stronger; the higher-order terms ignored in the derivation of the TLZ formula increase and the precession is no longer perfectly synchronized with the quadratic twist. We investigate the tunneling probability obtained at $m = 0.5 \text{ MHz}$ for a curvature range from $\kappa_{\parallel} = 0$ to $3 \mu\text{s}$. Figure 3(a iii) shows the experimental result, representing a clear nonreciprocal behavior to the speed F . As κ_{\parallel} increases, the PT condition approaches zero. A similar trend is observed in the TLZ formula shown in Fig. 3(a i), indicating that this characteristic is consistent with $F_{PT} = -\frac{2\Delta}{R_{12}(0)}$. This result proves that the speed of the quantum control is tunable by the geodesic curvature κ_{\parallel} of the driving field.

For a more quantitative comparison, we show a cross section at $\kappa_{\parallel} = 1.4 \mu\text{s}$ in Fig. 3(b i) [white line in Fig. 3(a iii)]. The experimental result (red circles) exhibits $P \sim 1$ near $F_{PT} = -0.045$ in good agreement with the TLZ formula (black solid line). On the other hand, in (negatively) large speeds $F < F_{PT}$, P decreases almost exponentially in the TLZ formula [24], whereas the change is gradual in the experimental result. This deviation becomes prominent as the gap parameter m and/or the curvature κ_{\parallel} are larger. The right panels of Figs. 3(a) and 3(b) show the corresponding data sets

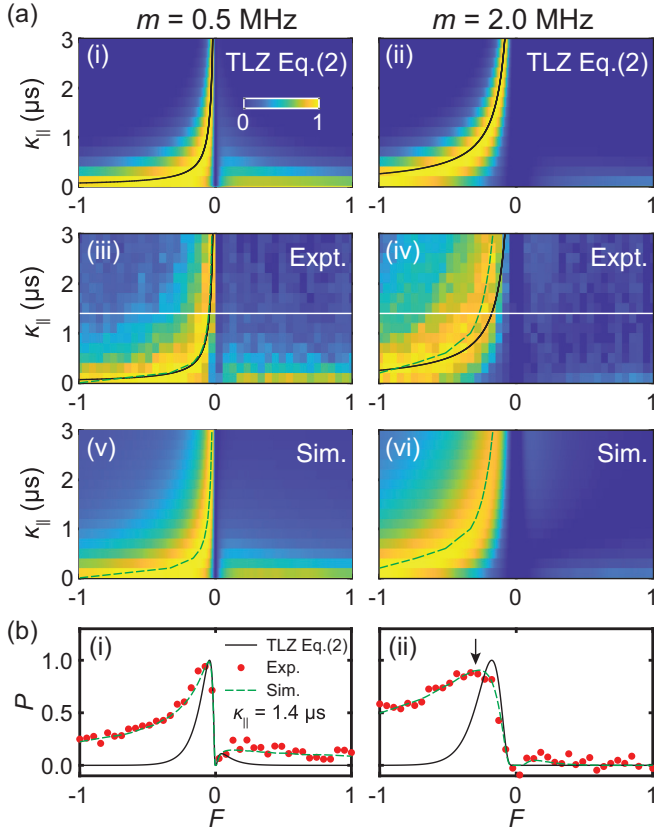


FIG. 3. Gap parameter and curvature dependence of the TLZ transition probability. (a) The left (right) panels denote the results at $m = 0.5$ MHz ($m = 2.0$ MHz). The black solid (green dashed) line indicates the PT condition in the TLZ formula (simulation). (b) Tunneling probability at $\kappa_{||} = 1.4$ μs [white line in (a i) and (a ii)]. The black arrow in (ii) indicates the PT condition.

obtained with a larger gap parameter ($m = 2.0$ MHz). The PT condition in the experiment (red circles) shifts to the left from what the TLZ formula (black solid line) predicts [black arrow in Fig. 3(b ii)]. The maximum P is then slightly suppressed from unity.

We obtain exact solutions by numerical simulations (see [35]) to discuss this deviation. The simulation results are in Figs. 3(a v) and 3(a vi) and the green dashed lines in Fig. 3(b). They reproduce the experimental results satisfactorily over the entire speed range. The black solid and green dashed lines in Fig. 3(a) show the perfect tunneling conditions obtained by the TLZ formula and the simulation, respectively. The results show that as the gap parameter m and curvature $\kappa_{||}$ become larger, the exact PT condition shifts toward the (negative) high speed side. Our precise measurements reveal that the higher-order terms are essential for a quantitative understanding of the TLZ transition.

As shown above, we find that nonreciprocity and high tunneling probability at finite speed always persist even when the TLZ formula is invalid. Thus, we conclude that these geometric effects are robust. Introducing a field twist can be a ubiquitous method of adjusting tunneling probabilities at arbitrary speeds, making the present TLZ model an alternative framework for quantum control at various energy scales. When applied to quantum materials, such control induces

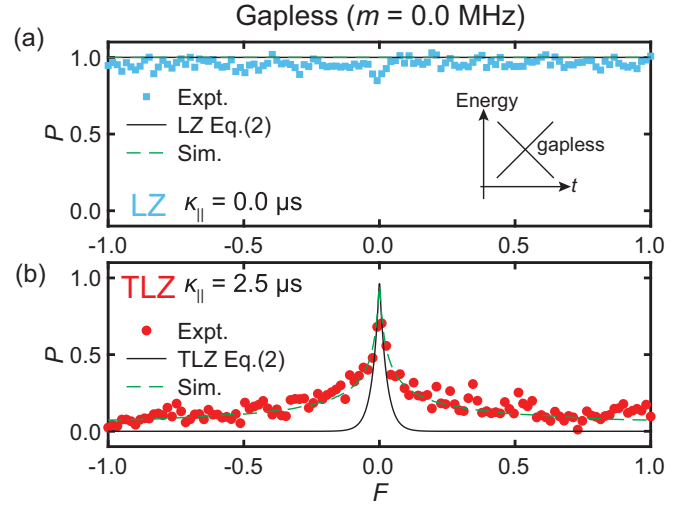


FIG. 4. Sweep speed dependence of the transition probability of the gapless ($m = 0.0$ MHz) system. (a) The LZ transition ($\kappa_{||} = 0$). The inset is a schematic of the energy change. (b) The TLZ transition ($\kappa_{||} = 2.5$ μs).

nontrivial properties such as the nonreciprocity of dc and photocurrent [24,25].

In the case of an infinitesimal gap ($m = 0.0$ MHz), the TLZ formula predicts a counterintuitive behavior, i.e., tunneling is suppressed as we increase the speed. Since this is relevant to the study of laser-field-driven dynamics in Dirac and Weyl semimetals [24], we study this situation in detail. The energy change is shown in the inset of Fig. 4(a), which mimics the situation where electrons in the valence band accelerated by the electric field are excited through the Dirac (Weyl) point into the conduction band. Here the LZ model and the TLZ model correspond to the case where the driving fields are dc and ac electric fields, respectively. We examine the LZ model and observe that it yields $P \sim 1$, as shown in Fig. 4(a). This is a straightforward phenomenon caused by the complete reversal of the field in the y axis. We then examine the TLZ transition at $\kappa_{||} = 2.5$ μs as in Fig. 4(b). The high tunneling probability near the adiabatic limit $F \sim 0$ is consistent with $F_{\text{PT}} = -\frac{4\pi m}{v\kappa_{||}} = 0$ (for $m = 0$). This behavior, where the probability decreases with increasing sweep speed, is opposite to the LZ transition at a finite gap [Fig. 2(b)]. This counterintuitive result is caused by the monocyclic nature of the quadratic twist, where the initial and final fields point in the same direction. It is qualitatively reproduced by the TLZ formula (black solid line) and is perfectly reproduced in the simulation (green dashed line).

We experimentally confirmed the nonadiabatic geometric effects of nonreciprocity and perfect tunneling in the quadratic TLZ model over a wide range of parameters. Specifically, we showed that we could utilize the geometric effects to control the quantum state dynamically. Geometric diabatic control can be applied to control systems of various energy scales, from nuclear spins to quantum materials. An important challenge to improving this method is to find a way to enhance the tunneling probability and bring it even closer to 100%. We think this is possible by engineering the shape of the field

twist to cancel the higher-order terms ignored in the derivation of the TLZ formula.

We thank K. M. Itoh (Keio University) for letting us use the confocal microscope system. This work is partially supported by “Advanced Research Infrastructure for Materials and Nanotechnology in Japan (ARIM)” of the Ministry of Education, Culture, Sports, Science and Technology (MEXT), Proposal No. JPMXP1222UT1131. This work was supported

by JSPS Grants-in-Aid for Scientific Research (Grants No. JP22K03524, No. JP19H00656, No. JP19H05826, No. JP23H01103, No. JP20H02187, and No. JP20H05661), JST CREST (Grants No. JPMJCR19T3 and No. JPMJCR1773), MEXT Q-LEAP (Grant No. JPMXS0118068379), JST Moonshot R&D (Grant No. JPMJMS2062), and MIC R&D for construction of a global quantum cryptography network (Grant No. JPMI00316), Next Generation Artificial Intelligence Research Center at the University of Tokyo.

-
- [1] F. Wilczek and A. Shapere, *Geometric Phases in Physics* (World Scientific, Singapore, 1989).
- [2] M. V. Berry and M. Wilkinson, Diabolical points in the spectra of triangles, *Proc. R. Soc. Lond. A* **392**, 15 (1984).
- [3] M. V. Berry, Geometric amplitude factors in adiabatic quantum transitions, *Proc. R. Soc. Lond. A* **430**, 405 (1990).
- [4] L. D. Landau, Zur theorie der energieübertragung II, *Phys. Z. Sow.* **2**, 46 (1932).
- [5] C. Zener, Non-adiabatic crossing of energy levels, *Proc. R. Soc. London Ser. A* **137**, 696 (1932).
- [6] E. C. G. Stückelberg, Theorie der unelastischen stöße zwischen atomen, *Helv. Phys. Acta* **5**, 369 (1932).
- [7] E. Majorana, Atomi orientati in campo magnetico variabile, *Nuovo Cim.* **9**, 43 (1932).
- [8] S. N. Shevchenko, S. Ashhab, and F. Nori, Landau-Zener-Stückelberg interferometry, *Phys. Rep.* **492**, 1 (2010).
- [9] O. V. Ivakhnenko, S. N. Shevchenko, and F. Nori, Nonadiabatic Landau-Zener-Stückelberg-Majorana transitions, dynamics, and interference, *Phys. Rep.* **995**, 1 (2023).
- [10] W. D. Oliver, J. Kim, R. C. Liu, and Y. Yamamoto, Hanbury Brown and Twiss-type experiment with electrons, *Science* **284**, 299 (1999).
- [11] J. R. Petta, H. Lu, and A. C. Gossard, A coherent beam splitter for electronic spin states, *Science* **327**, 669 (2010).
- [12] P. Huang, J. Zhou, F. Fang, X. Kong, X. Xu, C. Ju, and J. Du, Landau-Zener-Stückelberg Interferometry of a Single Electronic Spin in a Noisy Environment, *Phys. Rev. X* **1**, 011003 (2011).
- [13] J. Zhou, P. Huang, Q. Zhang, Z. Wang, T. Tan, X. Xu, F. Shi, X. Rong, S. Ashhab, and J. Du, Observation of Time-Domain Rabi Oscillations in the Landau-Zener Regime with a Single Electronic Spin, *Phys. Rev. Lett.* **112**, 010503 (2014).
- [14] S. Gasparinetti, P. Solinas, and J. P. Pekola, Geometric Landau-Zener Interferometry, *Phys. Rev. Lett.* **107**, 207002 (2011).
- [15] J. Zhang, J. Zhang, X. Zhang, and K. Kim, Realization of geometric Landau-Zener-Stückelberg interferometry, *Phys. Rev. A* **89**, 013608 (2014).
- [16] L. Wang, T. Tu, B. Gong, C. Zhou, and G.-C. Guo, Experimental realization of non-adiabatic universal quantum gates using geometric Landau-Zener-Stückelberg interferometry, *Sci. Rep.* **6**, 19048 (2016).
- [17] J.-d. Wu, M.-s. Zhao, J.-l. Chen, and Y.-d. Zhang, Adiabatic condition and quantum geometric potential, *Phys. Rev. A* **77**, 062114 (2008).
- [18] C. Xu, J. Wu, and C. Wu, Quantized interlevel character in quantum systems, *Phys. Rev. A* **97**, 032124 (2018).
- [19] D. Xiao, M.-C. Chang, and Q. Niu, Berry phase effects on electronic properties, *Rev. Mod. Phys.* **82**, 1959 (2010).
- [20] Q. Ma, A. G. Grushin, and K. S. Burch, Topology and geometry under the nonlinear electromagnetic spotlight, *Nat. Mater.* **20**, 1601 (2021).
- [21] D. N. Basov, R. D. Averitt, and D. Hsieh, Towards properties on demand in quantum materials, *Nat. Mater.* **16**, 1077 (2017).
- [22] J. Orenstein, J. E. Moore, T. Morimoto, D. H. Torchinsky, J. W. Harter, and D. Hsieh, Topology and symmetry of quantum materials via nonlinear optical responses, *Annu. Rev. Condens. Matter Phys.* **12**, 247 (2021).
- [23] A. de la Torre, D. M. Kennes, M. Claassen, S. Gerber, J. W. McIver, and M. A. Sentef, *Colloquium*: Nonthermal pathways to ultrafast control in quantum materials, *Rev. Mod. Phys.* **93**, 041002 (2021).
- [24] S. Takayoshi, J. Wu, and T. Oka, Nonadiabatic nonlinear optics and quantum geometry—Application to the twisted Schwinger effect, *SciPost Phys.* **11**, 075 (2021).
- [25] S. Kitamura, N. Nagaosa, and T. Morimoto, Nonreciprocal Landau-Zener tunneling, *Commun. Phys.* **3**, 63 (2020).
- [26] F. Gaitan, Temporal interferometry: A mechanism for controlling qubit transitions during twisted rapid passage with possible application to quantum computing, *Phys. Rev. A* **68**, 052314 (2003).
- [27] F. Gaitan, Controlling qubit transitions during non-adiabatic rapid passage through quantum interference, *J. Mod. Opt.* **51**, 2415 (2004).
- [28] R. Li, M. Hoover, and F. Gaitan, High-fidelity single-qubit gates using non-adiabatic rapid passage, *Quantum Inf. Comput.* **7**, 594 (2007).
- [29] R. Li and F. Gaitan, Robust high-fidelity universal set of quantum gates through non-adiabatic rapid passage, *J. Mod. Opt.* **58**, 1922 (2011).
- [30] J. W. Zwanziger, S. P. Rucker, and G. C. Chingas, Measuring the geometric component of the transition probability in a two-level system, *Phys. Rev. A* **43**, 3232 (1991).
- [31] D. Bouwmeester, G. P. Karman, N. H. Dekker, C. A. Schrama, and J. P. Woerdman, Observation of the geometric amplitude factor in an optical system, *J. Mod. Opt.* **43**, 2087 (1996).
- [32] D. Bouwmeester, G. P. Karman, C. A. Schrama, and J. P. Woerdman, Observation of interference in transitions due to local geometric phases, *Phys. Rev. A* **53**, 985 (1996).
- [33] J. W. Zwanziger, U. Werner-Zwanziger, and F. Gaitan, Non-adiabatic rapid passage, *Chem. Phys. Lett.* **375**, 429 (2003).

- [34] G. Fuchs, G. Burkard, P. Klimov, and D. Awschalom, A quantum memory intrinsic to single nitrogen-vacancy centres in diamond, *Nat. Phys.* **7**, 789 (2011).
- [35] See Supplemental Material at <http://link.aps.org/supplemental/10.1103/PhysRevA.107.053113> for details, which includes Refs. [38,39].
- [36] D. Misonou, K. Sasaki, S. Ishizu, Y. Monnai, K. M. Itoh, and E. Abe, Construction and operation of a tabletop system for nanoscale magnetometry with single nitrogen-vacancy centers in diamond, *AIP Adv.* **10**, 025206 (2020).
- [37] D. Guéry-Odelin, A. Ruschhaupt, A. Kiely, E. Torrontegui, S. Martínez-Garaot, and J. G. Muga, Shortcuts to adiabaticity: Concepts, methods, and applications, *Rev. Mod. Phys.* **91**, 045001 (2019).
- [38] V. Jacques, P. Neumann, J. Beck, M. Markham, D. Twitchen, J. Meijer, F. Kaiser, G. Balasubramanian, F. Jelezko, and J. Wrachtrup, Dynamic Polarization of Single Nuclear Spins by Optical Pumping of Nitrogen-Vacancy Color Centers in Diamond at Room Temperature, *Phys. Rev. Lett.* **102**, 057403 (2009).
- [39] A. Dréau, M. Lesik, L. Rondin, P. Spinicelli, O. Arcizet, J.-F. Roch, and V. Jacques, Avoiding power broadening in optically detected magnetic resonance of single NV defects for enhanced dc magnetic field sensitivity, *Phys. Rev. B* **84**, 195204 (2011).